RSC Advances

PAPER

View Article Online
View Journal | View Issue

Cite this: *RSC Adv.*, 2020, **10**, 40406

An orifice design: water insertion into C_{60}†

Yoshifumi Hashikawa, Kazuro Kizaki, Takashi Hirose and Yasujiro Murata *

Received 24th October 2020
Accepted 30th October 2020

DOI: 10.1039/d0ra09067k

rsc.li/rsc-advances

Using an open-cage C_{60} derivative possessing an orifice designed on the basis of computational studies, we have experimentally demonstrated the quantitative encapsulation of H_2O as well as effective conversion into $H_2O@C_{60}$ in an overall yield remarkably higher than the previously reported methods by *ca.* 2–5 times.

Soon after the discovery of C_{60},[1] the first endohedral fullerene, $K^+@C_{59}B$, was proven by Saunders and co-workers in 1991 under mass spectrometric conditions.[2] To date, a number of endohedral fullerenes encapsulating metal ions, nitrides, and oxides, which are so-called metallofullerenes, have been produced by physical approaches, *e.g.*, laser ablation and arc discharge methods.[3] While these approaches could provide endohedral fullerenes albeit only in 0.1% yield, their properties have received growing attention from a wide research area owing to their potential applications in photovoltaic cells ($Lu_3N@C_{80}$ (ref. 4) and $Li^+@C_{60}$ (ref. 5)) and MRI (magnetic resonance imaging) contrast agents ($Gd@C_{60}$ and $Gd@C_{82}$).[6] Additionally, DNP (dynamic nuclear polarization) was recently demonstrated by utilizing $Gd_2@C_{79}N$, which resulted in increased nuclear polarization of ^1H and ^{13}C spins from electron spins by *ca.* 50% at 1.2 K.[7]

In 1997, Rubin advocated an original concept to produce endohedral fullerenes *via* sequential steps: creation of an opening, insertion of small molecules, and closure of the opening.[8] This molecular surgical synthesis based on organic reactions is conceptually different from physical approaches. Of particular importance is to chemically synthesize endohedral fullerenes encapsulating neutral species that cannot be generated by physical approaches. Since the successful synthesis of the first open-cage C_{60} derivative in 1995 by Wudl and co-workers,[9] a number of derivatives with different structural motifs on their orifices have been reported.[10] In the present time, a variety of molecules have been found to be encapsulated inside the fullerene cavities, few of which are able to be restored into the pristine caged structures such as C_{60},[11] C_{70},[12] and $C_{59}N$[13] with retaining the molecule inside. Nevertheless, organic syntheses of such endohedral fullerenes still suffer from low yielding. To overcome this problem, we focused on an orifice structure which is crucial for trapping a guest molecule as well as for controlling the reactivity of open-cage C_{60} derivatives. Since the orifice substructure, *i.e.*, $^1ArC–E{=}C(^2Ar)–C(^3Ar)$, originates from a heterocyclic azine (Fig. 1) which is used for the creation of an opening by a thermal reaction with C_{60},[11c,14] we considered six hypothetical azines including pyridazines and triazines (**1a–f**) so as to design an orifice suitable both for encapsulation of guest molecules and closure of the opening. Herein, we discuss the molecular design toward efficient synthetic methodology for synthesizing endohedral fullerenes based on theoretical studies as well as experimental demonstration.

With regard to the synthesis of endohedral fullerenes, **INT1** (structure in Table 1) is a key material since it can encapsulate guest molecules such as H_2O,[11c] H_2,[15] and HF.[16] More importantly, the orifice with a substructure of tetraketone in **INT1** can be zipped up to reduce its orifice size from 16- to 8-membered ring by the reaction with phosphine and/or phosphite.[11c–e] The plausible mechanism on this closing process was depicted in

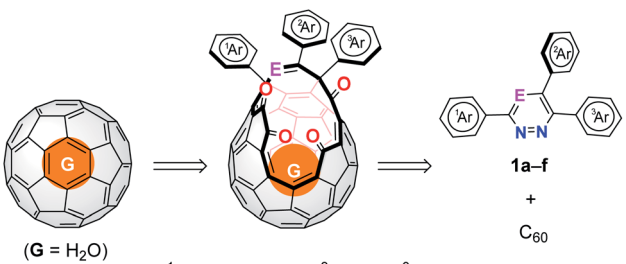

a : ^1Ar = Py, E = CH, ^2Ar = H , ^3Ar = Py
b : ^1Ar = Py, E = CH, ^2Ar = H , ^3Ar = Ph
c : ^1Ar = Py, E = CH, ^2Ar = Ph, ^3Ar = Ph
d : ^1Ar = Ph, E = CH, ^2Ar = H , ^3Ar = Ph
e : ^1Ar = Py, E = N , ^2Ar = H , ^3Ar = Ph
f : ^1Ar = Py, E = N , ^2Ar = Ph, ^3Ar = Ph

Fig. 1 Retrosynthetic route for endohedral fullerenes (Py: 2-pyridyl group).

Institute for Chemical Research, Kyoto University, Uji, Kyoto 611-0011, Japan. E-mail: yasujiro@scl.kyoto-u.ac.jp

† Electronic supplementary information (ESI) available: Detailed synthetic procedures, spectra, and optimized geometries. CCDC 1999283. For ESI and crystallographic data in CIF or other electronic format see DOI: 10.1039/d0ra09067k

Table 1 Partial charges q_{NPA} obtained by natural population analysis (NPA), stabilization energies $\Delta\Delta G$, and interatomic distances d (B3LYP-D3/6-31G(d) at 298 K)

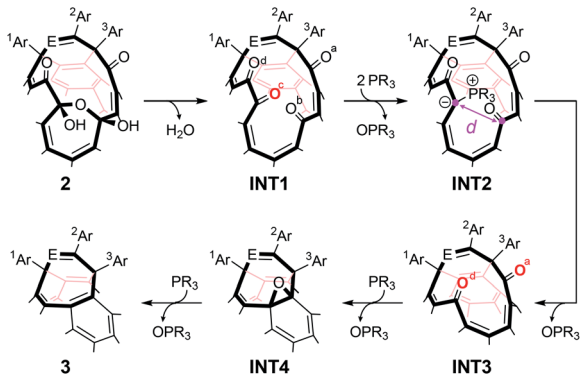

	q_{NPA}				
Addends	O(c)/**INT1**	O(a)/**INT3**	O(d)/**INT3**	$\Delta\Delta G$(**INT2**)[a] (kcal mol^{-1})	d(**INT2**) (Å)
a	−0.465	−0.510	−0.474	0.0	3.35
b	−0.464	−0.502	−0.469	−1.0	3.36
c	−0.467	−0.511	−0.467	+0.1	3.36
d	−0.461	−0.497	−0.469	−1.4	3.34
e	−0.465	−0.501	−0.469	−0.4	3.32
f	−0.464	−0.491	−0.469	−3.3	3.32

[a] $\Delta\Delta G$(**INT2**) = ΔG(**INT2**) − ΔG(**INT2a**) where ΔG(**INT2**) = G(**INT2**) + G($OPPh_3$) − G(**INT1**) − 2G(PPh_3).

Table 1. Firstly, a water molecule would be eliminated from the 13-membered ring of **2** to afford **INT1**. The ring-closing reaction is then initiated by the nucleophilic attack of PR_3 to O(c) in **INT1**, leading to the formation of β-oxo-phosphorus ylide **INT2** (ref. 17) which undergoes intramolecular Wittig reaction to give diketo derivative **INT3**.[18] The further nucleophilic attack of another PR_3 molecule on O(a) and/or O(d) in **INT3** followed by the elimination of O=PR_3 furnishes epoxide **INT4**.[19] Finally, deoxygenation of **INT4** by PR_3 provides **3** possessing an eight-membered-ring opening. Previously, we used **2a′** (which bears 6-*t*-butylpyridin-2-yl groups instead of 2-pyridyl groups) for preparing **INT2a′**. Even though **INT2a′** could be formed at 100 °C for 3 h, **INT2a′** was significantly decomposed during the conversion into **INT3a′** at 120 °C for 8 h, resulting in 52% yield.[20] Thus, open-cage C_{60} derivatives should have an orifice which meets criteria including (i) less polarized carbonyl groups in **INT1** and **INT3** to promote nucleophilic attack of PR_3 to carbonyl O-atoms, (ii) formation of stable ylide **INT2** to suppress undesirable decomposition pathways, and (iii) readily conversion of **INT2** into **INT3**.

To verify electronic and structural properties of **INT1**, **INT2**, and **INT3**, we performed theoretical calculations at the B3LYP-D3/6-31G(d) level of theory at 298 K (Table 1). From natural charges q_{NPA} of O(c) in **INT1**, the substituent effect is predicted to be not so significant in the initial step. Contrastingly, the q_{NPA} values of O(a) and O(d) in **INT3** are reflected by the opening substructure. Compared with **INT3a** which is a model that we previously synthesized,[11c] both absolute values of q_{NPA}, except for O(a) in **INT3c**, markedly decreased, suggestive of increased reactivity of **INT3** by replacing one of Py groups with a less electron-withdrawing Ph group at the ^{3}Ar position. Subsequently, we confirmed thermodynamic properties of β-oxo-phosphorus ylide **INT2**, showing considerable stabilization for **INT2f** ($\Delta\Delta G$ −3.3 kcal mol^{-1}) which is superior to others in preventing decomposition. This is probably due to the better orientation for one of Ph groups on the P-atom in **INT2f** *via* CH/π interaction with the Ph group at the ^{2}Ar position which is also tightly fixed *via* an H-bonding with the imine moiety (Fig. S8†). Furthermore, the replacement of an olefin unit with an imine moiety causes decrease in the C(b)···C(c) distance by 0.04 Å, implying the positive effect on the intramolecular Wittig reaction in **INT2e** and **INT2f**.

To gain insight into the orifice size of **INT1**, we summarized an energy profile for the H_2O-insertion as shown in Table 2. Interestingly, the H_2O-insertion is predicted to occur stepwisely. Firstly, the H_2O molecule is trapped at a cross-section of the orifice to form **INT5** *via* **TS1** which is the rate-determining step. Subsequently, the trapped H_2O molecule is encapsulated inside **INT1** *via* **TS2** to give H_2O@**INT1**. Upon seeing activation barriers, the Ph group at the ^{2}Ar position seems not to have considerable influence on the H_2O-insertion, showing the similar $\Delta G^{\ddagger}$ values of 21–22 kcal mol^{-1}. The substantial stabilization of **INT1f** by the H_2O encapsulation (ΔG −10.4 kcal mol^{-1}) would be an advantage to obstruct the escape of the H_2O molecule from the inside. Consequently, the orifice of **2f**, which consists of one Py and two Ph groups with an imine

Table 2 Changes in Gibbs energies (ΔG, kcal mol^{-1}) on a profile for H_2O-insertion into **INT1** (B3LYP-D3/6-31G(d) at 298 K)

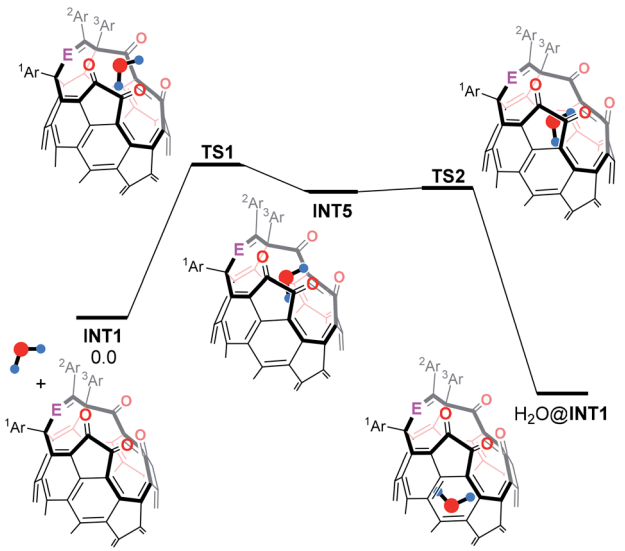

Addends	TS1	INT5	TS2	H_2O@INT1
a	+21.6	+17.1	+17.5	−10.0
b	+21.7	+17.2	+17.6	−9.3
c	+21.4	+16.9	+17.2	−8.9
d	+22.0	+17.5	+18.2	−9.7
e	+21.0	+17.3	+17.8	−8.9
f	+21.0	+17.3	+17.8	−10.4

moiety, should be preferable for the synthesis of $H_2O@C_{60}$ both in terms of reactivity on the closing process and capability of encapsulating a H_2O molecule.

Thereby, we synthesized **2f** by gram-scale reactions including the thermal reaction of C_{60} with 5,6-diphenyl-3-(pyridin-2-yl)-1,2,4-triazine (**1f**), photooxygenation,[14] and nucleophilic oxygenation using *N*-methylmorpholine *N*-oxide.[11c] Recently, we found that β-oxo-phosphorus ylide **INT2a′** bearing a PR_3 unit with a cone angle smaller than 140° is significantly hydrolysed in the presence of water.[17] As to the conversion from **INT3a′** to **3a′**, P(O*i*Pr)$_3$ was previously found to exhibit high performance.[18] For the efficient synthesis of $H_2O@C_{60}$, we designed one-pot reaction from **2f** to H_2O@**3f** *via* three steps commenced with the H_2O-insertion under high-pressure conditions followed by stepwise conversion of the thus formed H_2O@**2f** into H_2O@**INT3f** and then H_2O@**3f**. The results were summarized in Table 3. The H_2O-insertion was conducted using 20 mg of **2f** in a mixed solvent system of 1-chloronaphthalene (1-ClNp) and toluene under 9000 atm for 24 h. For the closure of the opening, we used PPh_3 with a cone angle of 145° (entry 1). Different from **2a′** that required totally 11 h for the conversion into **INT3a′**,[20] **2f** was transformed into **INT3f** within 1.5 to 2 h, meeting the criteria (i)–(iii) owing to stable ylide **INT2f** with a shorter C(b)⋯C(c) distance. The further reaction with P(O*i*Pr)$_3$ at 120 °C for 0.5 h gave desired H_2O@**3f** in 48% isolated yield with the encapsulation ratio of 98%. Whereas electron-deficient

Table 3 One-pot synthesis of H_2O@**3f** from **2f**[a]

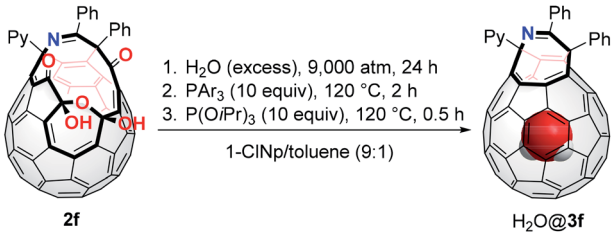

Entry	Step 1	Step 2	Yield[b]
1	160 °C	PPh_3	48% (H_2O: 98%)
2	160 °C	P(2-furyl)$_3$	21% (H_2O: 99%)
3	160 °C	P(*p*-tolyl)$_3$	69% (H_2O: 98%)
4	140 °C	P(*p*-tolyl)$_3$	67% (H_2O: 65%)
5	120 °C	P(*p*-tolyl)$_3$	68% (H_2O: 4%)

[a] Conducted using 20 mg of **2f** in a mixed solvent system of 1-chloronaphthalene (1-ClNp) and toluene. [b] Encapsulation ratio was determined by ^{1}H NMR or mass spectrum.

phosphine P(2-furyl)$_3$ gave H_2O@**3f** in lower yield (21%, entry 2), the reaction employing electron-rich P(*p*-tolyl)$_3$ resulted in higher yield (69%) with keeping the 98% encapsulation ratio of H_2O (entry 3). It should be noted that the decreased temperature at the first step drastically influenced on the encapsulation ratio of H_2O: 98% (160 °C, entry 3), 65% (140 °C, entry 4), and 4% (120 °C, entry 5).

The structure of H_2O@**3f** was determined spectroscopically. The molecular ion peak was observed at *m*/*z* 1020.1255 ([H_2O@**3f**]$^{\bullet-}$) in the negative ionization mode by the APCI (atmospheric-pressure chemical ionization) method. The ^{1}H NMR spectrum of H_2O@**3f** ($CDCl_3$, 500 MHz) clearly showed a singlet signal at δ −6.11 ppm corresponding to the

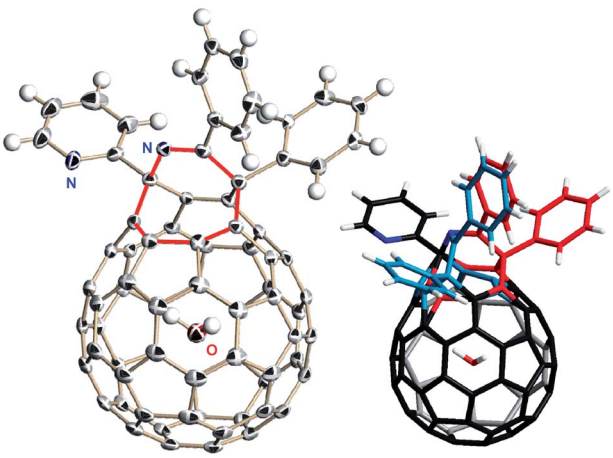

Fig. 2 Single crystal X-ray structure of H_2O@**3f** with showing thermal ellipsoids in 50% probability (left) and disordered structures coloured with pink and light blue for major and minor parts, respectively (right). The benzene molecules co-crystallized with H_2O@**3f** are omitted for clarity.

encapsulated H_2O molecule, bearing the striking resemblance with that for H_2O@**3a**′ (δ −6.09 ppm[11c,18]). Using H_2O@**3f** with an occupation level of 60%, single crystals were grown from the benzene/hexane solution by slow evaporation at 5 °C. The solid-state structure was shown in Fig. 2. The water molecule locates at the centre of the cage and its occupancy was refined to be 0.593(8), being in accordance with the ratio determined by ^{1}H NMR. A crystallographic disorder was seen in the orifice structure which is identical to two parts with sharing the Py group. Their occupancies were refined to be 0.854(2) for the major part and 0.146(2) for the minor part, respectively.

Based on our previous approach to synthesize $H_2O@C_{60}$ using **2a**′ in the solid state, the final step has the scale restriction up to 50 mg. Otherwise, the conversion is considerably decreased. For the scalable synthesis of $H_2O@C_{60}$, we examined one-pot synthesis of $H_2O@C_{60}$ using 160 mg of **2f**. As represented in Scheme 1, **2f** was firstly subjected to the optimal reaction conditions as entry 3 in Table 3. To the resultant mixture, methanol was added to obtain the crude precipitate containing H_2O@**3f** which was further heated at 400 °C under 5 Pa for 2 h, giving $H_2O@C_{60}$ in 6% isolated yield. Considering the high conversion of **2f** into H_2O@**3f** (Table 3), H_2O@**3f** should be mostly decomposed during the final step. To avoid undesirable decomposition pathways, the crude mixture was purified, prior to step 4, by silica gel column chromatography which gave H_2O@**3f** (80% yield) together with complex mixture having higher polarity. Since this complex mixture changed into insoluble solid without formation of $H_2O@C_{60}$ under the same conditions as step 4, it might hamper the conversion of H_2O@**3f** into $H_2O@C_{60}$. With H_2O@**3f** as a pure form in hand, it was subjected to pyrolytic conditions (Scheme 1). As the results, $H_2O@C_{60}$ was obtained up to 87% yield and the overall yield from **2f** reaches to 70% which is remarkably higher than that obtained by our previous approach (15% from **2a**′)[11c] even when compared with Whitby's variant (40% from **2a**′).[15]

In summary, we designed the orifice substructure suitable for the synthesis of endohedral fullerenes on the basis of reactivity toward closing processes and encapsulation properties. Among six candidates, the orifice possessing a phenyl imine moiety (**f**) was expected to have high affinity to phosphines as well as interaction with the encapsulated H_2O molecule, which is strong enough to prevent its escape from the inside. The thus synthesized open-cage C_{60} derivative **2f** demonstrated the effective conversion into H_2O@**3f** *via* one-pot process, showing high yield up to 80% with nearly quantitative encapsulation of H_2O. The further conversion of H_2O@**3f** into $H_2O@C_{60}$ proceeded quite well when H_2O@**3f** was used in a pure form. The method demonstrated herein could be applied for a variety of endohedral fullerenes in a practical scale.

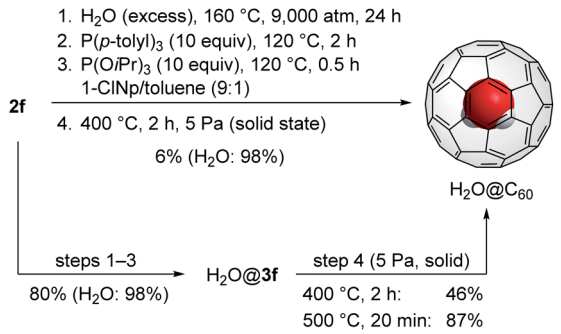

Scheme 1 Synthesis of $H_2O@C_{60}$ from **2f** (160 mg).

Conflicts of interest

There are no conflicts to declare.

Acknowledgements

Financial support was partially provided by the JSPS KAKENHI Grant Number JP17H06119 and JP18K14200. We thank Dr Kyusun Kim for the initial trials on the synthesis of **2f**.

Notes and references

1 H. W. Kuroto, J. R. Heath, S. C. O'Brien, R. F. Curl and R. E. Smalley, *Nature*, 1985, **318**, 162–163.
2 Y. Chai, T. Guo, C. Jing, R. E. Haufler, L. P. F. Chibante, J. Fure, L. Wang, J. M. Alford and R. E. Smalley, *J. Phys. Chem.*, 1991, **95**, 7564–7568.
3 (*a*) A. Rpdríguez-Fortea, A. L. Balch and J. M. Poblet, *Chem. Soc. Rev.*, 2011, **40**, 3551–3563; (*b*) A. A. Popov, S. Yang and L. Dunsch, *Chem. Rev.*, 2013, **113**(8), 5989–6113.
4 R. B. Ross, C. M. Cardona, D. M. Guldi, S. G. Sankaranarayanan, M. O. Reese, N. Kopidakis, J. Peet, B. Walker, G. C. Bazan, E. V. Keuren, B. C. Holloway and M. Drees, *Nat. Mater.*, 2009, **8**, 208–212.
5 I. Jeon, H. Ueno, S. Seo, K. Aitola, R. Nishikubo, A. Saeki, H. Okada, G. Boschloo, S. Maruyama and Y. Matsuo, *Angew. Chem., Int. Ed.*, 2018, **57**, 4607–4611.
6 K. B. Ghiassi, M. M. Olmstead and A. L. Balch, *Dalton Trans.*, 2014, **43**, 7346–7358.
7 X. Wang, J. E. McKay, B. Lama, J. v. Tol, T. Li, K. Kirkpatrick, Z. Gan, S. Hill, J. R. Long and H. C. Dorn, *Chem. Commun.*, 2018, **54**, 2425–2428.
8 Y. Rubin, *Chem. – Eur. J.*, 1997, **3**, 1009–1016.
9 J. C. Hummelen, M. Prato and F. Wudl, *J. Am. Chem. Soc.*, 1995, **117**, 7003–7004.
10 (*a*) M. Murata, Y. Murata and K. Komatsu, *Chem. Commun.*, 2008, 6083–6094; (*b*) G. C. Vougioukalakis, M. M. Roubelakis and M. Orfanopoulos, *Chem. Soc. Rev.*, 2010, **39**, 817–844; (*c*) L. Shi and L. Gan, *J. Phys. Org. Chem.*, 2013, **26**, 766–772.
11 (*a*) K. Komatsu, Y. Murata and Y. Murata, *Science*, 2005, **307**, 238–240; (*b*) Y. Morinaka, F. Tanabe, M. Murata, Y. Murata and K. Komatsu, *Chem. Commun.*, 2010, **46**, 4532–4534; (*c*) K. Kurotobi and Y. Murata, *Science*, 2011, **333**, 613–616; (*d*) A. Krachmalnicoff, R. Bounds, S. Mamone, S. Alom, M. Concistrè, B. Meier, K. Kouřil, M. E. Light, M. R. Johnson, S. Rols, A. J. Horsewill, A. Shugai, U. Nagel, T. Rõõm, M. Carravetta, M. H. Levitt and R. J. Whitby, *Nat. Chem.*, 2016, **8**, 953–957; (*e*) S. Bloodworth, G. Sitinova, S. Alom, S. Vidal, G. R. Bacanu, S. J. Elliott, M. E. Light, J. M. Herniman, G. J. Langley, M. H. Levitt and

R. J. Whitby, *Angew. Chem., Int. Ed.*, 2019, **58**, 5038–5043; (*f*) S. Bloodworth, G. Hoffman, M. C. Walkey, G. R. Bacanu, J. M. Herniman, M. H. Levitt and R. J. Whitby, *Chem. Commun.*, 2020, **56**, 10521–10524.

12 (*a*) M. Murata, S. Maeda, Y. Morinaka, Y. Murata and K. Komatsu, *J. Am. Chem. Soc.*, 2008, **130**, 15800–15801; (*b*) R. Zhang, M. Murata, T. Aharen, A. Wakamiya, T. Shimoaka, T. Hasegawa and Y. Murata, *Nat. Chem.*, 2016, **8**, 435–441; (*c*) R. Zhang, M. Murata, A. Wakamiya and Y. Murata, *Sci. Adv.*, 2017, **3**, e1602833; (*d*) Y. Morinaka, R. Zhang, S. Sato, H. Nikawa, T. Kato, K. Furukawa, M. Yamada, Y. Maeda, M. Murata, A. Wakamiya, S. Nagase, T. Akasaka and Y. Murata, *Angew. Chem., Int. Ed.*, 2017, **56**, 6488–6491.

13 (*a*) Y. Hashikawa, M. Murata, A. Wakamiya and Y. Murata, *J. Am. Chem. Soc.*, 2016, **138**, 4096–4104; (*b*) Y. Hashikawa, M. Murata, A. Wakamiya and Y. Murata, *J. Org. Chem.*, 2017, **82**, 4465–4469; (*c*) Y. Hashikawa and Y. Murata, *J. Am. Chem. Soc.*, 2017, **139**, 18468–18471; (*d*) G.-Z. Zhu, Y. Liu, Y. Hashikawa, Q.-F. Zhang, Y. Murata and L.-S. Wang, *Chem. Sci.*, 2018, **9**, 5666–5671.

14 Y. Murata, M. Murata and K. Komatsu, *Chem. – Eur. J.*, 2003, **9**, 1600–1609.

15 A. Krachmalnicoff, M. H. Levitt and R. J. Whitby, *Chem. Commun.*, 2014, **50**, 13037–13040.

16 A. Krachmalnicoff, R. Bounds, S. Mamone, M. H. Levitt, M. Carravetta and R. J. Whitby, *Chem. Commun.*, 2015, **51**, 4993–4996.

17 Y. Hashikawa, S. Okamoto and Y. Murata, *Commun. Chem.*, 2020, **3**, 90.

18 Y. Hashikawa, M. Murata, A. Wakamiya and Y. Murata, *J. Am. Chem. Soc.*, 2017, **139**, 16350–16358.

19 Y. Hashikawa, H. Yasui, K. Kurotobi and Y. Murata, *Mater. Chem. Front.*, 2018, **2**, 206–213.

20 Y. Hashikawa and Y. Murata, *Chem. Lett.*, 2020, **49**, 244–247.